STATISTICS, OPTIMIZATION AND INFORMATION COMPUTING
Stat., Optim. Inf. Comput., Vol. **16**, December 2026, pp 5761–5775.
Published online in International Academic Press (www.IAPress.org)

Geometric optimal control for the second-order synchronous-machine model

Andrés Felipe Camelo Muñoz, Carlos Alberto Ramírez Vanegas, Guillermo Villa Martínez*

afkamelo@utp.edu.co, caramirez@utp.edu.co, gvilla@utp.edu.co
Department of Mathematics, Universidad Tecnológica de Pereira, Colombia

Abstract This paper studies the transient regulation problem for the classical second-order synchronous-machine infinite-bus model from the viewpoint of geometric optimal control. The swing dynamics are formulated as a nonlinear affine-in-control system on a cylindrical state space, where the rotor-angle dynamics and the speed deviation are coupled through a sinusoidal electrical power relation. After recalling the local linearization around a synchronous operating point, the discussion is connected with the classical equal-area criterion in order to interpret first-swing stability in geometric terms. The control problem is then reformulated on the cotangent bundle by means of Pontryagin's Maximum Principle, leading to a canonical Hamiltonian system whose extremals determine the optimal mechanical-power and damping-type control actions. A fault scenario is incorporated through a piecewise variation of the transferable power, and the resulting two-point boundary value problem is solved numerically by a collocation-based method. The simulations provide the power–angle curves, optimal control profiles, state responses, and phase portraits, showing how the Hamiltonian extremal steers the machine from a pre-fault operating regime toward a desired post-fault synchronous state while penalizing control effort and state deviations. In this way, the paper connects classical transient-stability concepts with a geometric optimal-control framework for the regulated swing equation.

Keywords synchronous machine, swing equation, transient stability, geometric control, boundary value problem.

AMS 2010 subject classifications 49K15, 93C10, 93C15, 34H05.

DOI: 10.19139/soic-2310-5070-4775

1. Introduction

Transient stability is a central issue in power-system operation because severe disturbances may drive synchronous generators away from their nominal operating conditions and, in extreme cases, lead to loss of synchronism [1, 3, 5]. This problem becomes particularly relevant after short circuits, switching events, or abrupt changes in power transfer, where the electromechanical response of the machine must remain bounded while the system evolves toward a new post-fault operating regime.

For single-machine infinite-bus configurations, the classical second-order swing equation remains one of the most widely used models for transient-stability analysis. Despite its reduced order, this model captures the essential nonlinear interaction between mechanical input power, electrical air-gap power, inertia, damping, and rotor-angle motion. In particular, the electrical power term

$$P_e = P_{\max} \sin \delta$$

introduces the main nonlinearity of the model and determines the restoring effect that competes with rotor acceleration during transient conditions [4, 5].

*Correspondence to: Guillermo Villa Martínez (Email: gvilla@utp.edu.co). Department of Mathematics, Universidad Tecnológica de Pereira, Carrera 27 #10-02 Barrio Alamos - Pereira - Risaralda - Colombia (660003).

ISSN 2310-5070 (online) ISSN 2311-004X (print)
Copyright © 2026 International Academic Press

Traditional transient-stability studies often rely on local linearization around an equilibrium point or on qualitative criteria such as the equal-area method. These approaches are useful for interpretation and preliminary assessment, but they do not provide a direct framework for selecting control actions that drive the generator toward a desired post-fault synchronous state while maintaining acceptable control effort and satisfactory dynamic performance. Recent studies have investigated complementary nonlinear-control strategies for second-order electromechanical models and power-electronic systems. These approaches include phase-portrait-based stability analysis combined with generalized backstepping control, exact feedback linearization followed by decoupled PI regulation, and passivity-based control strategies for current-source converters [13, 14, 15]. Collectively, these contributions provide a relevant framework for the analysis of nonlinear stability and the design of controllers in electromechanical and power-conversion applications. This paper addresses that question by formulating the second-order synchronous-machine model as a nonlinear control system and then posing a finite-horizon optimal control problem for transient regulation. The state of the machine is given by

$$x(t) = \begin{pmatrix} \omega(t) \\ \delta(t) \end{pmatrix},$$

where ω is the speed deviation with respect to the synchronous reference and δ is the rotor angle. The controlled swing dynamics are described by

$$\begin{cases} \dot{\omega} = \dfrac{1}{M}\big(P_m - P_{\max}\sin(\delta) - \xi\,\omega\big), \\ \dot{\delta} = \omega, \end{cases} \tag{1}$$

where $M > 0$ is the inertia constant, P_m denotes the mechanical-power action, and ξ represents a damping-type control channel. In this way, the model incorporates both the physical swing dynamics and the possibility of active transient regulation [4, 6].

A first objective of the paper is to rewrite (1) in a form suitable for nonlinear control analysis. To this end, the system is expressed as an affine-in-control dynamics on the state manifold $\mathbb{R} \times \mathbb{S}^1$:

$$\dot{x} = f(x) + g_1(x)\,u_1 + g_2(x)\,u_2, \qquad u_1 = P_m, \quad u_2 = \xi. \tag{2}$$

This representation separates the intrinsic nonlinear machine dynamics from the available actuation channels and provides the appropriate setting for optimal-control design, phase-space interpretation, and transient analysis under constraints [4, 5, 6]. A second objective is to connect the nonlinear formulation with the standard local analysis used in power engineering. Around a synchronous operating point (ω_0, δ_0) [4, 5], defined by

$$\omega_0 = 0, \qquad P_{m0} = P_{\max}\sin(\delta_0),$$

the model can be linearized to obtain a small-signal approximation. Introducing the perturbation variables

$$\Delta\omega = \omega - \omega_0, \qquad \Delta\delta = \delta - \delta_0,$$

the local dynamics take the form

$$\begin{bmatrix} \Delta\dot{\omega} \\ \Delta\dot{\delta} \end{bmatrix} = A_0 \begin{bmatrix} \Delta\omega \\ \Delta\delta \end{bmatrix}, \qquad A_0 = \begin{bmatrix} -\dfrac{\xi}{M} & -\dfrac{P_{\max}}{M}\cos(\delta_0) \\ 1 & 0 \end{bmatrix}. \tag{3}$$

This local model is useful for interpreting the equilibrium behavior and relating the proposed formulation to classical small-signal stability concepts. However, because the transient regime considered here is generated by a fault and involves nonlinear excursions, the local model alone is not sufficient for the regulation problem studied in this work.

For that reason, the main development of the paper is based on the full nonlinear dynamics. The transient-regulation problem is posed as an optimal control problem in which the machine is required to move from a

pre-fault equilibrium toward a desired post-fault synchronous state while penalizing both state deviations and control effort. The resulting formulation is developed through Pontryagin's Maximum Principle, which leads to a Hamiltonian boundary-value problem whose solution determines the optimal transient-control actions.

From an application viewpoint, the contribution of the paper is to combine three complementary levels of analysis within a single framework: the physical swing-equation model, the classical transient-stability interpretation through energy considerations, and an optimal-control formulation capable of generating regulated post-fault trajectories. The numerical experiment illustrates this idea under a fault scenario by computing the state response, the optimal control profiles, the power–angle curves, and the phase portrait associated with the regulated transient.

1.1. Notation

Throughout the paper, the state manifold is denoted by

$$\mathcal{M} = \mathbb{R} \times \mathbb{S}^1.$$

The machine state is

$$x(t) = (\omega(t), \delta(t))^\top,$$

where ω is the speed deviation and δ is the rotor angle. The inertia constant is denoted by $M > 0$, the mechanical input by P_m, the damping-type input by ξ, and the electrical air-gap power by

$$P_e = P_{\max} \sin \delta.$$

The affine-in-control representation is written in terms of the drift and input vector fields f, g_1, and g_2. The operating point for local analysis is (ω_0, δ_0), and the perturbation variables are $\Delta\omega$ and $\Delta\delta$. The matrix A_0 denotes the Jacobian matrix of the linearized system.

In the optimal-control problem, the initial and terminal states are

$$x_0 = (0, \delta_0), \qquad x_1 = (0, \delta_1),$$

the running-cost weights are $k_\omega > 0$ and $k_\delta > 0$, the desired rotor angle is δ_d, and the final time is T_f. The admissible bounds are denoted by $P_m^{\max}$ and $\xi_{\max}$. On the cotangent bundle $T^*\mathcal{M}$, we use canonical coordinates

$$q = (\omega, \delta), \qquad p = (p_\omega, p_\delta).$$

The PMP Hamiltonian is denoted by $\mathcal{H}(x, p; P_m, \xi)$, the maximized Hamiltonian by $H(x, p)$, and the reconstructed optimal controls by $P_m^*(t)$ and $\xi^*(t)$. For the transient-stability analysis, $E(\omega, \delta)$ denotes the mechanical energy, A_1 and A_2 the acceleration and deceleration areas in the equal-area criterion, δ_s and δ_u the post-fault stable and unstable equilibrium angles, and Γ_{cr} the critical clearing curve. Finally, $J[P_m, \xi]$ denotes the continuous Bolza functional, J_h its discrete approximation, N the number of mesh nodes, and t_{fault}, t_{clear} the fault inception and clearing times.

1.2. Organization

The paper is organized as follows. Section 2 formulates the optimal-control problem for the swing equation, derives its Hamiltonian representation, extends the model to first-order governor dynamics, and relates the proposed approach to equal-area and energy-function methods. Section 3 presents the numerical experiment for a fault scenario, including the computational procedure, the control reconstruction, and the resulting power–angle curves, control profiles, state trajectories, and phase portrait. Finally, Section 4 discusses possible extensions toward multimachine systems and more realistic structure-preserving control formulations.

2. From Stabilization to Optimal Geometric Control

The local linearization (3) provides a useful description of the generator dynamics in a neighborhood of the synchronous operating point, but transient regulation after a severe disturbance requires a nonlinear formulation. In practical terms, the problem is not only to determine whether the machine remains stable after a fault, but also to identify control actions that guide the system toward a desired post-fault operating condition with limited effort and acceptable dynamic behavior [1, 3, 5].

This motivates the transition from a classical stabilization viewpoint to an optimal-control formulation. In the present setting, the transient is influenced by two control channels: the mechanical-power action P_m and a damping-type action ξ. The purpose of the control design is to use these inputs to steer the generator from a pre-fault synchronous condition to a target post-fault equilibrium while accounting for actuator limitations and penalizing large deviations in angle and speed.

2.1. Optimal control formulation on the swing model

We consider the controlled swing dynamics in affine-in-control form,

$$\dot{x} = f(x) + g_1(x)\, P_m + g_2(x)\, \xi, \qquad x = \begin{pmatrix} \omega \\ \delta \end{pmatrix} \in \mathcal{M}, \tag{4}$$

with drift and input vector fields

$$f(\omega,\delta) = \begin{pmatrix} -\dfrac{P_{\max}}{M}\sin\delta \\ \omega \end{pmatrix}, \qquad g_1(\omega,\delta) = \begin{pmatrix} \dfrac{1}{M} \\ 0 \end{pmatrix}, \qquad g_2(\omega,\delta) = \begin{pmatrix} -\dfrac{\omega}{M} \\ 0 \end{pmatrix}.$$

This decomposition makes the control problem operationally transparent: the drift f describes the natural nonlinear electromechanical evolution of the machine, while g_1 and g_2 indicate how the available control actions modify that evolution [1, 2, 3].

To obtain a regulated post-fault transient, we define the performance index

$$J[P_m,\xi] = \Phi\big(x(T_f)\big) + \frac{1}{2}\int_0^{T_f} \Big(P_m^2 + \xi^2 + k_\omega\,\omega^2 + k_\delta(\delta-\delta_d)^2\Big)\, dt \to \min, \tag{5}$$

subject to the controlled dynamics (4), the boundary conditions

$$x(0) = x_0 = (0,\delta_0), \qquad x(T_f) = x_1 = (0,\delta_1),$$

and the admissible bounds

$$|P_m| \le P_m^{\max}, \qquad |\xi| \le \xi_{\max}.$$

The terms P_m^2 and ξ^2 penalize excessive control effort, while the weighted state terms $k_\omega\omega^2$ and $k_\delta(\delta-\delta_d)^2$ penalize deviations from the desired synchronous regime. Thus, the regulation objective is encoded explicitly in the optimization problem. The terminal term $\Phi(x(T_f))$ is retained for generality, although in the numerical experiment the terminal state is fixed, so $\Phi(x(T_f))$ reduces to an additive constant and does not affect the optimality conditions.

The selected running cost represents a compromise between transient regulation and control effort. The terms P_m^2 and ξ^2 discourage excessively large mechanical-power and damping-type actions, whereas $k_\omega\omega^2$ penalizes speed deviations and $k_\delta(\delta-\delta_d)^2$ promotes convergence toward the desired post-fault rotor angle. Therefore, k_ω and k_δ determine the relative importance assigned to speed regulation and angular tracking. The quadratic form was selected because it provides a physically interpretable objective and leads to a Hamiltonian that is strictly concave with respect to the control variables. Consequently, the unconstrained optimal controls admit explicit reconstruction formulas in terms of the state and costate variables. Different choices of the objective would modify the resulting control structure. Larger penalties on control effort would reduce the magnitude of the optimal actions, whereas larger state-deviation weights would generally produce a more aggressive regulation response. A nonconstant

terminal penalty would modify the costate terminal conditions. Moreover, nonsmooth control penalties, such as L^1-type terms, could produce sparse or nonsmooth controls, while a minimum-time objective with bounded controls would typically favor saturated or bang–bang actions.

To compute the optimal transient, we apply Pontryagin's Maximum Principle and define the Hamiltonian

$$\mathcal{H}(x,p;P_m,\xi) = p_\omega \frac{1}{M}\Big(P_m - P_{\max}\sin\delta - \xi\,\omega\Big) + p_\delta\,\omega - \frac{1}{2}\Big(P_m^2 + \xi^2 + k_\omega\omega^2 + k_\delta(\delta-\delta_d)^2\Big), \tag{6}$$

where $p=(p_\omega,p_\delta)$ is the costate vector associated with the state variables (ω,δ). The PMP converts the original transient-regulation problem into a two-point boundary value problem involving the state and costate variables.

The canonical equations are

$$\dot q = \frac{\partial \mathcal{H}}{\partial p}, \qquad \dot p = -\frac{\partial \mathcal{H}}{\partial q},$$

together with the pointwise maximization condition

$$(P_m^*(t),\xi^*(t)) \in \arg\max_{(P_m,\xi)\in\mathcal{U}} \mathcal{H}(x(t),p(t);P_m,\xi), \qquad \text{for a.e. } t\in[0,T_f].$$

Therefore, once the state–costate trajectory is determined, the corresponding optimal control inputs can be reconstructed directly.

2.1.1. Unconstrained optimal controls When the control bounds are inactive, maximization of (6) with respect to P_m and ξ yields

$$P_m^* = \frac{p_\omega}{M}, \qquad \xi^* = -\frac{p_\omega\,\omega}{M}. \tag{7}$$

These expressions are convenient for numerical implementation because they provide explicit formulas for the control signals in terms of the state–costate variables.

2.1.2. Hamiltonian state–costate dynamics Substituting (7) into the canonical equations, the extremals satisfy

$$\dot\omega = \frac{\partial H}{\partial p_\omega} = \frac{1}{M}\Big(P_m^* - P_{\max}\sin\delta - \xi^*\,\omega\Big), \qquad \dot\delta = \frac{\partial H}{\partial p_\delta} = \omega, \tag{8}$$

$$\dot p_\omega = -\frac{\partial H}{\partial \omega} = \frac{\xi^*}{M}\,p_\omega - p_\delta + k_\omega\,\omega, \tag{9}$$

$$\dot p_\delta = -\frac{\partial H}{\partial \delta} = \frac{P_{\max}}{M}\,p_\omega\cos\delta + k_\delta(\delta-\delta_d). \tag{10}$$

From an engineering viewpoint, this system provides the mechanism through which the optimal transient is computed. The state variables describe the generator response, the costate variables encode the sensitivity of the performance index, and the reconstructed inputs determine the regulation effort required to obtain the desired post-fault trajectory. The preceding formulation constitutes the core model used in the numerical study. The following governor-augmented model is included as a conceptual extension that illustrates how finite actuator dynamics may be incorporated into the same geometric framework.

2.2. Extension with first-order governor dynamics

The classical second-order formulation treats the mechanical power P_m as a direct control action. Although this assumption is useful for exposing the geometric structure of the transient-regulation problem, actual mechanical-power variations are produced through turbine and governor dynamics and therefore cannot occur instantaneously. A first extension of the model is obtained by introducing a first-order governor response:

$$\begin{cases} \dot\omega = \dfrac{1}{M}\left(P_m - P_{\max}\sin\delta - \xi\omega\right), \\ \dot\delta = \omega, \\ T_g\dot P_m = -P_m + P_m^{\mathrm{ref}} + u_g, \end{cases} \tag{11}$$

where $T_g > 0$ is the governor time constant, P_m^{ref} is the reference mechanical-power level, and u_g denotes the governor command. The extended state is

$$x_e = (\omega, \delta, P_m)^\top,$$

while the control variables are u_g and ξ. The corresponding performance index may be written as

$$\begin{aligned} J_e[u_g, \xi] &= \Phi_e\big(x_e(T_f)\big) \\ &\quad + \frac{1}{2}\int_0^{T_f} \Big[r_g u_g^2 + \xi^2 + k_\omega \omega^2 + k_\delta(\delta - \delta_d)^2 + k_m(P_m - P_m^{\mathrm{ref}})^2\Big]\, dt, \end{aligned} \tag{12}$$

where $r_g > 0$ penalizes governor effort and $k_m > 0$ penalizes mechanical-power deviations. Using the costate vector

$$p_e = (p_\omega, p_\delta, p_m),$$

the PMP Hamiltonian becomes

$$\begin{aligned} \mathcal{H}_e &= \frac{p_\omega}{M}\left(P_m - P_{\max}\sin\delta - \xi\omega\right) + p_\delta \omega \\ &\quad + \frac{p_m}{T_g}\left(-P_m + P_m^{\mathrm{ref}} + u_g\right) \\ &\quad - \frac{1}{2}\Big[r_g u_g^2 + \xi^2 + k_\omega \omega^2 + k_\delta(\delta - \delta_d)^2 + k_m(P_m - P_m^{\mathrm{ref}})^2\Big]. \end{aligned} \tag{13}$$

When the control constraints are inactive, the pointwise maximization condition gives

$$u_g^* = \frac{p_m}{T_g r_g}, \qquad \xi^* = -\frac{p_\omega \omega}{M}. \tag{14}$$

The additional costate equation associated with the mechanical-power state is

$$\dot{p}_m = -\frac{p_\omega}{M} + \frac{p_m}{T_g} + k_m(P_m - P_m^{\mathrm{ref}}). \tag{15}$$

The equations for p_ω and p_δ retain the same structure as in the second-order formulation. This extension demonstrates that the geometric optimal-control framework can incorporate finite actuator dynamics while preserving an affine-in-control representation. The governor time constant introduces a dynamic limitation on mechanical-power regulation and prevents the instantaneous actuation assumed in the reduced model. The numerical experiment considered in this work remains based on the classical second-order system in order to isolate its Hamiltonian structure, while the numerical investigation of the extended governor model is left for future work. After presenting this extension, the remainder of the paper returns to the classical second-order model in order to isolate its Hamiltonian structure and numerical behavior.

2.3. Classical transient-stability interpretation

Before analyzing the controlled transient, it is useful to recall the standard energy-based interpretation of the uncontrolled swing equation. For a severe disturbance such as a short circuit, the equal-area criterion provides a practical way to assess first-swing stability without solving the full nonlinear dynamics explicitly [4, 6].

Assume that a fault occurs at $t = t_f$ and reduces the electrical transfer capability to a fault-on characteristic $P_e^f(\delta)$, followed by fault clearing at $t = t_{\mathrm{cl}}$ and restoration to a post-fault characteristic $P_e^{pf}(\delta)$. If the machine initially operates at the pre-fault equilibrium, then during the fault the electrical output decreases and the rotor accelerates. The associated acceleration area is

$$A_1 = \int_{\delta_0}^{\delta_{\mathrm{cl}}} \left(P_m - P_e^f(\delta)\right) d\delta.$$

After clearing, if the post-fault electrical power exceeds the mechanical input, the rotor decelerates and the corresponding deceleration area is

$$A_2 = \int_{\delta_{\mathrm{cl}}}^{\delta_{\max}} \left(P_e^{pf}(\delta) - P_m\right) d\delta.$$

The equal-area criterion states that first-swing stability is maintained if the kinetic energy gained during acceleration can be compensated by the decelerating effect after fault clearing. In practical terms, this criterion gives an intuitive interpretation of the fault transient and helps identify critical clearing conditions. However, it does not prescribe a control action; it only characterizes the qualitative post-fault behavior of the uncontrolled system.

For the purposes of this work, the equal-area criterion serves as an interpretive tool. It clarifies the physical meaning of the transient and provides a bridge between classical power-system analysis and the optimal-control formulation developed here. In particular, it shows how the fault modifies the energy balance, while the optimal-control problem determines how the available actuation can be used to improve the post-fault response.

2.4. Phase-plane viewpoint and role of control

The nonlinear character of the swing equation can also be interpreted through the phase plane (δ, ω). In the uncontrolled post-fault regime, the machine dynamics admit the mechanical-energy representation

$$E(\omega, \delta) = \frac{1}{2} M\omega^2 + V(\delta), \qquad V(\delta) = -\int^{\delta} (P_m - P_e(s))\, ds.$$

This representation helps identify stable and unstable equilibrium points and the associated separatrix that bounds the post-fault stability region. From this viewpoint, the critical clearing state is the one that remains inside the admissible energy boundary of the post-fault system.

More specifically, if $(0, \delta_s)$ denotes the post-fault stable equilibrium, determined by

$$P_m = P_{\max}^{\mathrm{pf}} \sin(\delta_s), \qquad 0 < \delta_s < \frac{\pi}{2},$$

then the corresponding unstable equilibrium is

$$(0, \delta_u), \qquad \delta_u = \pi - \delta_s.$$

The separatrix associated with $(0, \delta_u)$ defines the boundary of the post-fault attraction region, and the critical clearing curve may be interpreted as the set of clearing states whose energy coincides with that boundary.

Phase-portrait analysis has also been employed to examine the open- and closed-loop stability of nonlinear electromechanical systems and to show how nonlinear feedback can alter the qualitative behavior of their equilibrium points [13].

The controlled problem extends this picture. Instead of accepting the post-fault transient as a purely passive response, the proposed formulation uses the control channels P_m and ξ to shape the evolution of the system. The goal is not only to preserve synchronism, but also to improve the quality of the transient by reducing deviations and limiting the cost of regulation [4, 6].

This interpretation links the physical and computational aspects of the problem. On the one hand, the equal-area criterion and the phase-plane description explain how the generator behaves under a disturbance. On the other hand, the Hamiltonian formulation explains how the controlled transient can be computed as the solution of an optimization problem. The numerical experiment developed later should therefore be understood as a regulated transient-stability study: the machine response is not merely observed after the fault, but actively driven toward a desired synchronous post-fault state according to an optimality criterion [4, **?**, 12].

In this sense, the proposed framework combines physical interpretability and control design. The classical swing equation provides the underlying generator model, the equal-area and phase-plane viewpoints provide the transient-stability interpretation, and the optimal-control problem provides the mechanism for computing admissible control actions that improve the post-fault response [**?**, 12].

2.5. Comparison with classical transient-stability methods

The equal-area criterion, energy-function methods, and geometric optimal control address complementary aspects of transient stability. The equal-area criterion assesses first-swing stability by comparing the accelerating and

decelerating energy contributions and may be used to estimate critical clearing conditions. Energy-function methods characterize stability margins through energy levels and the separatrix associated with the post-fault attraction region. However, neither method directly synthesizes corrective control actions.

Table 1 summarizes the main differences.

Table 1. Comparison of transient-stability approaches.

Method	**Purpose**	**Main output**	**Control synthesis**
Equal-area criterion	First-swing stability assessment	Energy-area balance and critical clearing condition	No
Energy-function method	Stability-margin characterization	Critical energy level and separatrix	No
Geometric optimal control	Finite-horizon transient regulation	Optimal state–costate trajectory and control profiles	Yes

Control synthesis may be approached through several nonlinear design paradigms. Recent studies have considered exact feedback linearization combined with decoupled PI regulation for second-order nonlinear systems, as well as IDA-PBC, nonlinear PI, and PI-PBC strategies for electrical power converters [14, 15]. These methods construct feedback laws through nonlinear transformations, passivity principles, or energy-shaping arguments. In contrast, the present approach formulates a finite-horizon optimal-control problem, computes the associated state–costate extremal, and reconstructs the control actions through Pontryagin's Maximum Principle.

The connection with the energy-function viewpoint can be expressed through the post-fault reference energy

$$E_{\mathrm{pf}}(\omega,\delta)=\frac{1}{2}M\omega^2+\int_{\delta_s}^{\delta}\left(P_e^{\mathrm{pf}}(s)-P_m^{\mathrm{ref}}\right)\,ds, \tag{16}$$

where P_m^{ref} is the mechanical-power level associated with the post-fault equilibrium. Along a controlled post-fault trajectory,

$$\dot{E}_{\mathrm{pf}}=\left(P_m-P_m^{\mathrm{ref}}\right)\omega-\xi\omega^2. \tag{17}$$

Equation (17) shows how the controls modify the classical energy balance. The mechanical-power action may inject or remove energy, whereas a positive damping action dissipates energy through $-\xi\omega^2$. In the uncontrolled reference case, $P_m=P_m^{\mathrm{ref}}$ and $\xi=0$, the post-fault energy is conserved on each autonomous interval.

Thus, the equal-area and energy-function approaches provide stability assessment and physical interpretation, while the geometric formulation determines control actions that steer the system toward a prescribed post-fault state. The three approaches should therefore be regarded as complementary rather than competing.

3. Numerical experiment

We now illustrate the indirect geometric-control formulation associated with the Bolza functional (5). The experiment is posed on the swing manifold

$$\mathcal{M}=\mathbb{R}\times\mathbb{S}^1,$$

while the extremals are computed on the cotangent bundle $T^*\mathcal{M}$ through the canonical state–costate dynamics (8)–(10). The controls are reconstructed pointwise from the unconstrained maximizer (7). Hence, the numerical problem is to determine an integral curve of the maximized Hamiltonian vector field satisfying the prescribed boundary conditions [3].

Since the parameter set is application-dependent, we keep the notation

$$M,\quad P_{\max},\quad k_\omega,\quad k_\delta,\quad \delta_d,\quad T_f,\quad \delta_0,\quad \delta_1,\quad P_m^{\max},\quad \xi_{\max}$$

explicit throughout the experiment. The initial and terminal states are taken as

$$x(0)=(0,\delta_0),\qquad x(T_f)=(0,\delta_1).$$

Accordingly, the state–costate trajectory is computed as a two-point boundary value problem, with the boundary conditions imposed at $t=0$ and $t=T_f$.

Substituting (7) into (8)–(10), the maximized Hamiltonian dynamics become

$$\dot{\omega} = \frac{1}{M}\left(\frac{p_\omega}{M} - P_{\max}\sin\delta + \frac{p_\omega \omega^2}{M}\right), \qquad \dot{\delta} = \omega, \tag{18}$$

$$\dot{p}_\omega = \frac{\xi^*(t)}{M}p_\omega - p_\delta + k_\omega\omega, \qquad \dot{p}_\delta = \frac{P_{\max}}{M}p_\omega\cos\delta + k_\delta(\delta - \delta_d). \tag{19}$$

The corresponding control reconstruction is

$$P_m^*(t) = \frac{p_\omega(t)}{M}, \qquad \xi^*(t) = -\frac{p_\omega(t)\omega(t)}{M}. \tag{20}$$

Here the terminal term $\Phi(x(T_f))$ in (5) is retained for generality. In the present numerical experiment, however, the terminal state is fixed, so that $\Phi(x(T_f))$ reduces to an additive constant and does not affect the optimality conditions.

For the simulations reported below, the inertia constant is fixed at $M = 5.0$, while the weights in the running cost are chosen as

$$k_\omega = 5.0, \qquad k_\delta = 20.0.$$

The final time is taken as $T_f = 10$, and the reference operating level is set to

$$P_m^{\mathrm{ref}} = 0.8.$$

This value is used to define the pre-fault and post-fault operating regimes, but it is not imposed as a constant control along the extremal. The fault scenario is introduced through the switching times

$$t_{\mathrm{fault}} = 1.0, \qquad t_{\mathrm{clear}} = 1.2.$$

Accordingly, the equilibrium angles associated with the reference operating level are

$$\delta_0 = \arcsin\left(\frac{0.8}{1.20}\right) \approx 0.7297, \qquad \delta_1 = \arcsin\left(\frac{0.8}{1.00}\right) \approx 0.9273,$$

and the desired angular value in the cost functional is chosen as

$$\delta_d = \delta_1.$$

In the implementation, if the values in (20) leave the admissible box constraints, they are projected onto

$$[-P_m^{\max}, P_m^{\max}] \qquad \text{and} \qquad [-\xi_{\max}, \xi_{\max}],$$

respectively. This preserves admissibility while retaining the Hamiltonian interpretation of the unconstrained extremal as the reference flow [8, 9, 10].

Once an admissible extremal is obtained, the performance index is approximated by

$$J_h = \Phi(x(T_f)) + \frac{1}{2}\sum_{j=0}^{N-1}\left[\left(P_m^*(t_j)\right)^2 + \left(\xi^*(t_j)\right)^2 + k_\omega\omega(t_j)^2 + k_\delta\left(\delta(t_j) - \delta_d\right)^2\right]\Delta t, \tag{21}$$

which is the discrete counterpart of the Bolza functional (5).

From the geometric viewpoint, the experiment tracks a Hamiltonian extremal on $T^*\mathcal{M}$, whereas its projection onto $\mathcal{M}$ gives the physical evolution of the generator. The state variables (ω, δ) describe the motion on the cylinder, while the covector (p_ω, p_δ) selects the optimal actuation through the maximization rule. In particular, the term $-p_\delta$ in (19) is essential: it transfers the angular covector component into the ω-channel and therefore cannot be omitted without altering the canonical Hamiltonian flow [3].

To evaluate the numerical solution, we report the terminal errors

$$|\omega(T_f)|, \qquad |\delta(T_f) - \delta_1|,$$

the discrete cost J_h, and the fractions of time for which the controls hit their bounds. Since the fault is modeled through a piecewise time-dependent profile $P_{\max}(t)$, the Hamiltonian is not globally autonomous across the switching instants; therefore, Hamiltonian preservation can only be interpreted on each autonomous subinterval [3].

3.1. Computational procedure

Algorithm 1 Boundary-value algorithm for the numerical experiment

Require: M, k_ω, k_δ, T_f, $P_{\max}^{\mathrm{pre}}$, $P_{\max}^{\mathrm{fault}}$, $P_{\max}^{\mathrm{post}}$, t_{fault}, t_{clear}, P_m^{ref}, N, tolerance ε

Ensure: Approximations of $\omega(t)$, $\delta(t)$, $p_\omega(t)$, $p_\delta(t)$, the reconstructed controls $P_m^*(t)$, $\xi^*(t)$, the discrete cost J_h, and the graphical outputs

1: Define the piecewise transfer profile

$$P_{\max}(t) = \begin{cases} P_{\max}^{\mathrm{pre}}, & 0 \le t < t_{\mathrm{fault}}, \\ P_{\max}^{\mathrm{fault}}, & t_{\mathrm{fault}} \le t < t_{\mathrm{clear}}, \\ P_{\max}^{\mathrm{post}}, & t_{\mathrm{clear}} \le t \le T_f \end{cases}$$

2: Compute

$$\delta_0 = \arcsin\left(\frac{P_m^{\mathrm{ref}}}{P_{\max}^{\mathrm{pre}}}\right), \qquad \delta_1 = \arcsin\left(\frac{P_m^{\mathrm{ref}}}{P_{\max}^{\mathrm{post}}}\right), \qquad \delta_d = \delta_1$$

3: Construct a uniform mesh $t_j = j\Delta t$ on $[0, T_f]$, where $\Delta t = T_f/N$

4: Impose the boundary conditions

$$\omega(0) = 0, \qquad \delta(0) = \delta_0, \qquad \omega(T_f) = 0, \qquad \delta(T_f) = \delta_1$$

5: Choose an initial guess on the mesh

$$\omega^{(0)}(t_j) = 0, \qquad \delta^{(0)}(t_j) = \delta_0 + \frac{t_j}{T_f}(\delta_1 - \delta_0),$$

$$p_\omega^{(0)}(t_j) = M\, P_m^{\mathrm{ref}}, \qquad p_\delta^{(0)}(t_j) = 0$$

6: Solve the boundary value problem (18)–(19) by a collocation method

7: Reconstruct the controls at each node:

$$P_m^*(t_j) = \frac{p_\omega(t_j)}{M}, \qquad \xi^*(t_j) = -\frac{p_\omega(t_j)\omega(t_j)}{M}$$

8: If needed, project the controls onto

$$P_m^*(t_j) \in [-P_m^{\max}, P_m^{\max}], \qquad \xi^*(t_j) \in [-\xi_{\max}, \xi_{\max}]$$

9: Approximate the discrete cost by (21)

10: Evaluate the terminal errors

$$|\omega(T_f)|, \qquad |\delta(T_f) - \delta_1|$$

11: Generate the power–angle diagram, the control profiles, the state responses, and the phase portrait in the (δ, ω)-plane

The numerical results reported below are obtained by solving the two-point boundary value problem associated with (18)–(19). Rather than using a shooting method, the computation is carried out by a collocation-based boundary value solver on a prescribed temporal mesh. The fault is incorporated through the piecewise profile $P_{\max}(t)$, so that the same Hamiltonian framework remains valid before, during, and after the disturbance. Once the state–costate trajectory has been computed, the controls are reconstructed pointwise from (20), and the discrete cost and graphical outputs are evaluated on a refined temporal grid. This choice is consistent with recent numerical developments on constrained optimal control and collocation-based discretization methods [8, 9, 10, 11].

In the numerical implementation, the boundary value problem is solved on a uniform mesh with $N = 600$ nodes on $[0, T_f]$, using a collocation solver with tolerance 10^{-5} and at most 30000 mesh nodes. The initial guess is taken as

$$\omega^{(0)}(t) = 0, \qquad \delta^{(0)}(t) = \delta_0 + \frac{t}{T_f}(\delta_1 - \delta_0), \qquad p_\omega^{(0)}(t) = MP_m^{\mathrm{ref}}, \qquad p_\delta^{(0)}(t) = 0.$$

After convergence, the numerical extremal is evaluated on a refined grid of 2000 time points in order to reconstruct the controls $P_m^*(t)$ and $\xi^*(t)$, compute the electrical power

$$P_e(t) = P_{\max}(t) \sin \delta(t),$$

and generate the power–angle, control, state-response, and phase-plane plots [8, 9].

The preceding algorithm summarizes the computational realization of the Hamiltonian extremal associated with the indirect optimal-control formulation. Its output is precisely the family of curves displayed in Figures 1–4, which provide the observable signature of the geometric regulation mechanism on the physical state manifold.

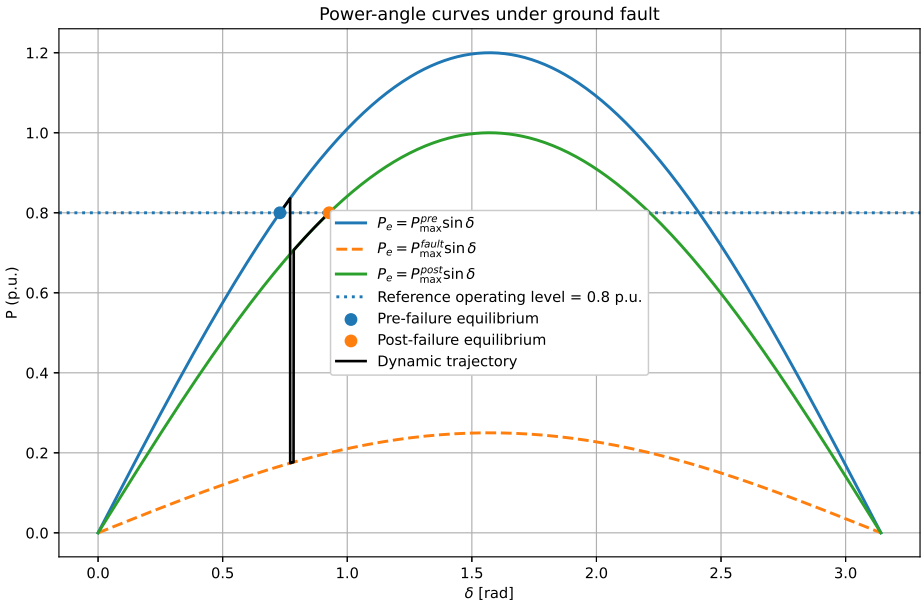


Figure 1. Power vs angle curves before, during, and after the ground fault.

Figure 1 depicts the power–angle curves in the pre-fault, fault-on, and post-fault regimes, together with the dynamic trajectory of the machine. The temporary drop in $P_{\max}$ during the fault reduces the electrical transfer capability and forces the trajectory away from the pre-fault equilibrium. After clearing, the post-fault characteristic guides the system toward the desired synchronous regime, consistently with the geometric optimal-control formulation [4, 6].

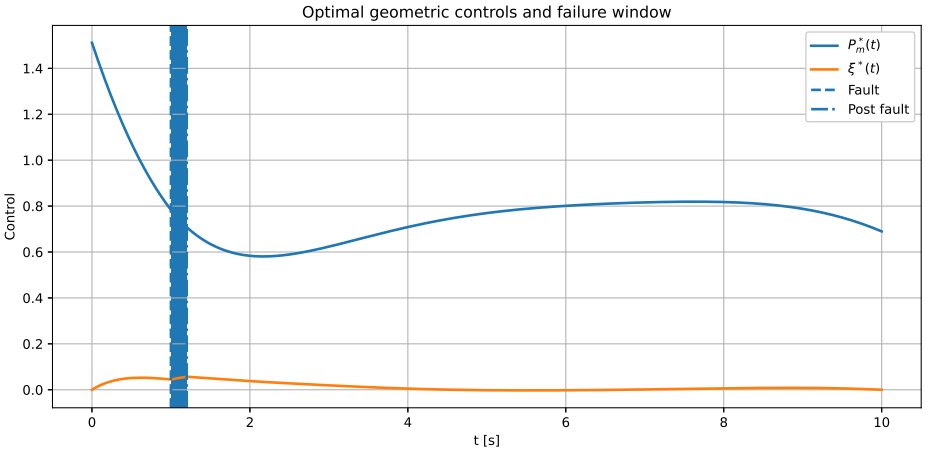


Figure 2. Optimal geometric controls $P_m^*(t)$ and $\xi^*(t)$, showing the fault inception and clearing times.

Figure 2 shows the optimal controls $P_m^*(t)$ and $\xi^*(t)$ during the fault scenario. Their variation near the fault inception and clearing instants reflects the optimal corrective action needed to mitigate the disturbance and recover the desired synchronous operating regime. In geometric terms, these curves are the control components induced by the Hamiltonian extremal associated with the transient regulation problem [3].

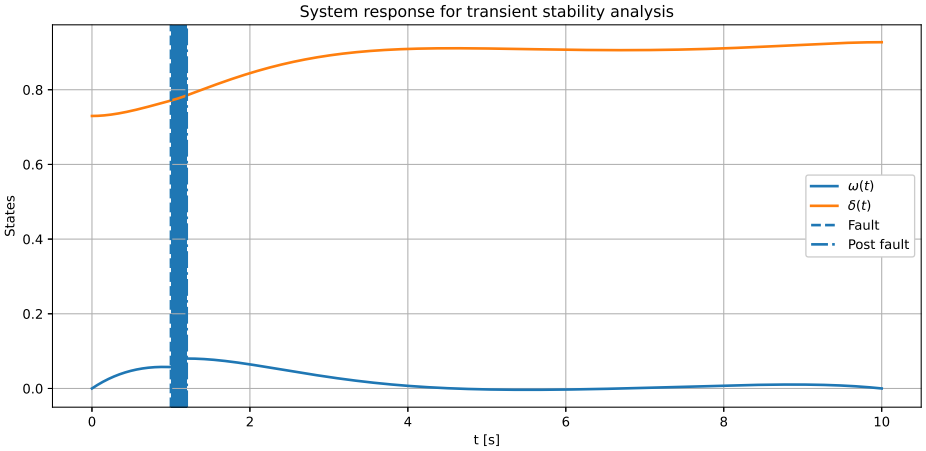


Figure 3. Time response of the state variables for transient-stability analysis.

Figure 3 represents the temporal evolution of $\omega(t)$ and $\delta(t)$ under the fault scenario. The state deviation induced by the disturbance is followed by a regulated post-fault response that drives the machine toward the desired synchronous operating condition. In this sense, the figure illustrates the transient-stability behavior produced by the geometric optimal-control formulation [4, 5].

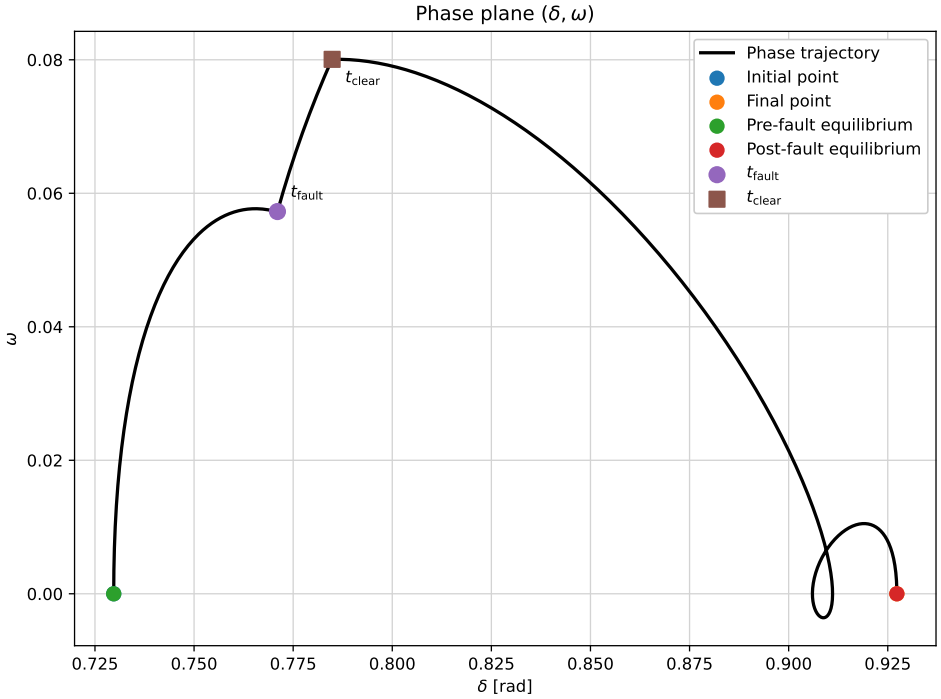


Figure 4. Phase plane (δ, ω) showing the system trajectory.

Figure 4 shows the trajectory of the machine in the (δ, ω)-plane during the fault and post-fault stages. The marked points t_{fault} and t_{clear} identify the main transition in the transient response, while the trajectory evolves from the pre-fault equilibrium toward the post-fault synchronous regime. In geometric terms, this phase portrait is the projection of the Hamiltonian extremal and summarizes the controlled transient-stability behavior of the system [3].

3.2. Additional disturbance scenarios

To assess the proposed formulation under different operating conditions, four additional numerical scenarios are considered. The cases vary the fault-on transfer capability, clearing time, inertia constant, and reference mechanical-power level. These parameters influence the disturbance severity, the duration of rotor acceleration, and the resulting control effort.

Table 2 summarizes the parameters used in each scenario.

Table 2. Parameters of the additional numerical scenarios.

Case	$\boldsymbol{P_{\max}^{\text{fault}}}$	$\boldsymbol{t_{\text{clear}}}$	$\boldsymbol{M}$	$\boldsymbol{P_m^{\text{ref}}}$
1	0.20	1.10	5.0	0.8
2	0.05	1.20	5.0	0.8
3	0.05	1.35	4.0	0.8
4	0.05	1.20	5.0	0.9

For each scenario, the regulated transient is evaluated through the peak speed deviation, the maximum post-fault angular deviation, the discrete cost, and the maximum amplitudes of the optimal controls:

$$\max_{t\in[0,T_f]} |\omega(t)|, \qquad \max_{t\in[t_{\text{clear}},T_f]} |\delta(t) - \delta_d|.$$

The resulting performance indicators are reported in Table 3.

Table 3. Performance indicators for the numerical scenarios.

Case	$\max \lvert\omega\rvert$	$\max_{t \geq t_{\mathrm{clear}}} \lvert\delta - \delta_d\rvert$	J_h	$\max \lvert P_m^* \rvert$	$\max \lvert\xi^*\rvert$
1	0.075282	0.147691	3.688662	1.526622	0.056832
2	0.082759	0.143599	3.631768	1.501464	0.057460
3	0.102386	0.126598	3.529169	1.492501	0.057698
4	0.116613	0.191133	5.005892	1.931530	0.091428

The peak speed deviation increases from Cases 1 to 3 as the disturbance becomes more severe through reduced fault-on transfer capability, delayed clearing, and lower inertia. However, the control amplitudes and the performance index do not vary monotonically because they depend on the complete optimal trajectory and on the trade-off between regulation and control effort. Case 4 yields the largest speed deviation, control amplitudes, and cost, indicating that operation closer to the power-transfer limit has the most significant effect among the conditions considered.

The numerical experiments developed here should be interpreted as an indirect geometric optimal-control analysis of the transient regulation problem for the classical second-order synchronous-machine infinite-bus model subject to a fault. The computed curves in Figures 1–4 do not represent a purely uncontrolled post-fault evolution; instead, they are the projection onto the physical state manifold of a Hamiltonian extremal on $T^*\mathcal{M}$, together with the controls reconstructed from the maximization condition. Consequently, the experiment provides a transient-stability study from a geometric-control perspective, in the sense that it quantifies how the machine may be driven from the pre-fault equilibrium toward a desired post-fault synchronous regime while penalizing both control effort and state deviations. This interpretation is more precise than a purely classical stability statement, since the present framework emphasizes optimal transient regulation rather than the sole qualitative assessment of the uncontrolled swing equation [3, 4, 8].

4. Future work

The present work focuses on a second-order single-machine infinite-bus model and shows how the transient regulation problem can be formulated and computed within an indirect geometric optimal-control framework. A natural continuation is to extend this perspective to multimachine systems, where the coupling between generators, network constraints, and fault propagation leads to a substantially richer geometric structure [6, 7].

- A first direction is about controller design, future work should also address the geometric description of transient-stability boundaries in multimachine systems. Recent differential-geometric approaches suggest that the shape of the stability region may be characterized through geometric objects associated with the power-flow manifold [7]. Connecting these ideas with the optimal-control framework developed here could provide a more complete description of both transient regulation and stability margins [4, 5].
- A second extension is the development of multimachine formulations based on port-Hamiltonian structure. Since the present model already admits a Hamiltonian interpretation on the cotangent bundle, it is natural to investigate whether the same geometric ideas can be embedded into structure-preserving port-Hamiltonian descriptions of power networks [6]. This would allow the transient regulation problem to be studied together with the intrinsic energy exchange between generators and transmission lines.

Finally, from a computational viewpoint, it would be of interest to combine the present indirect approach with reduced-order models, LPV formulations, or sensitivity-based geometric indicators, as well as with FACTS devices and inverter-based resources. Such developments would move the present study from a conceptual single-machine setting toward realistic multimachine environments, in which geometric control may provide a unified framework for transient stability, optimal regulation, and robustness under large disturbances [7, 8, 9].

The numerical implementation and validation of the governor-augmented model introduced in Subsection 2.1.2 constitute a direct continuation of this study. Further extensions may incorporate excitation-system dynamics, turbine stages, actuator saturation, and parameter uncertainty. These additions would increase the dimension of the Hamiltonian boundary-value problem and require additional physical parameters and time constants.

Acknowledgement

This work was supported by Grupo de Investigación en Matemática Aplicada y Educación at Universidad Tecnológica de Pereira.

REFERENCES

1. Mnif, Faical. *Differential-geometric normal forms and structure-preserving control of single-input underactuated Euler–Lagrange systems under disturbances*, International Journal of Dynamics and Control, vol. 14(3), pp. 91, 2026.
2. Kvalheim, Matthew D. and Koditschek, Daniel E. *Necessary conditions for feedback stabilization and safety*, Journal of Geometric Mechanics, vol. 14, no. 4, pp. 659–693, 2022. DOI: 10.3934/jgm.2022013.
3. Sachkov, Yuri. *Introduction to Geometric Control*, Springer Optimization and Its Applications, Springer, Cham, 2022. DOI: 10.1007/978-3-031-02070-4.
4. Chaudhary, Rekha and Singh, Arun Kumar. *Transient Stability Improvement of Power System Using Non-Linear Controllers*, Energy and Power Engineering, 6(1), 10–16, 2014. DOI: 10.4236/epe.2014.61002.
5. Arif, Jawad, Ray, Swakshar, and Chaudhuri, Balarko. *MIMO Feedback Linearization Control for Power Systems*, International Journal of Electrical Power & Energy Systems, 45(1), 87–97, 2013. DOI: 10.1016/j.ijepes.2012.08.051.
6. Irfan, M., Kulkarni, S., Kulkarni, P., Wagh, S., and Singh, N. M. *Transient Stability Improvement of Multi-machine Power System using Higher Order Sliding Mode Control*, IFAC Proceedings Volumes, 47(1), 1054–1060, 2014. DOI: 10.3182/20140313-3-IN-3024.00134.
7. Wu, Dan, Wolter, Franz-Erich, and Geng, Sijia. *Approximating Voltage Stability Boundary Under High Variability of Renewables Using Differential Geometry*, Electric Power Systems Research, 236, Article 110716, 2024. DOI: 10.1016/j.epsr.2024.110716.
8. Zhao, Bowen, Xu, Honglei, and Teo, Kok Lay. *A numerical algorithm for constrained optimal control problems*, Journal of Industrial and Management Optimization, vol. 19, no. 12, pp. 8602–8616, 2023. DOI: 10.3934/jimo.2023053.
9. Su, Shuxuan, Shao, Mengzhen, Yu, Changjun, and Teo, Kok Lay. *On the correlation of local collocation and control parameterization methods*, Journal of Industrial and Management Optimization, vol. 20, no. 7, pp. 2329–2357, 2024. DOI: 10.3934/jimo.2024004.
10. Alioua, Imane and Bibi, Mohand Ouamer. *Method for solving the norm in an optimal control problem*, Numerical Algebra, Control and Optimization, vol. 15, no. 4, pp. 1066–1091, 2025. DOI: 10.3934/naco.2025002.
11. Abadia-Doyle, Gabriela, Hager, William W., and Rao, Anil V. *Integral form of Legendre-Gauss-Lobatto collocation for optimal control*, Journal of the Franklin Institute, vol. 363, no. 1, article 108120, 2026. DOI: 10.1016/j.jfranklin.2025.108120.
12. Krishan, Ram and Verma, Ashu. *Assessment and Enhancement of Hopf Bifurcation Stability Margin in Uncertain Power Systems*, Electric Power Systems Research, vol. 206, article 107783, 2022. DOI: 10.1016/j.epsr.2022.107783.
13. Montoya Giraldo, Oscar Danilo, Ramírez Vanegas, Carlos Alberto, and Mesa, Fernando. *A phase-portrait stability analysis for a reaction wheel pendulum using a generalized backstepping control approach*, Statistics, Optimization & Information Computing, vol. 13, no. 2, pp. 474–487, 2024. DOI: 10.19139/soic-2310-5070-2164.
14. Montoya Giraldo, Oscar Danilo, Gil-González, Walter Julián, and Jutinico-Alarcón, Andrés. *A Decoupled PI Design for a Second-Order Model of a Magnetic Levitation System*, Statistics, Optimization & Information Computing, vol. 14, no. 2, pp. 628–635, 2025. DOI: 10.19139/soic-2310-5070-2390.
15. Nivia-Vargas, Ang, Montoya Giraldo, Oscar Danilo, and Gil-González, Walter Julián. *Comparative Analysis of Control Strategies for Single-Phase PWM-CSCs Feeding Linear Loads: IDA-PBC, Nonlinear PI, and PI-PBC Approaches*, Statistics, Optimization & Information Computing, vol. 14, no. 3, pp. 1337–1355, 2025. DOI: 10.19139/soic-2310-5070-2410.